



# The Quest to reliable structure-activity relationships on heterogeneous catalysts in methanol steam reforming

Research report for the Marshall Plan Scholarship

**Kevin Ploner, MSc**

Department of Physical Chemistry, University of Innsbruck

Innrain 52c, 6020 Innsbruck, Austria

Supervisor at home university:

Priv.-Doz. Dr. Simon Penner

Supervisor at host university:

Dr. Martin Kunz

Lawrence Berkeley National Laboratory, Advanced Light Source

1 Cyclotron Road, Berkeley, CA 94720-8229, USA

# Table of contents

1. Abstract
2. Results
  - 2.1 Original goals and research problems
    - 2.1.1 Scientific background
    - 2.1.2 Redesign of the MSR setup
    - 2.1.3 In situ XRD investigations of Cu-In samples in MSR
  - 2.2 Changes and deviations
  - 2.3 Summary of obtained results
    - 2.3.1 MSR setup
    - 2.3.2 In situ XRD studies
      - 2.3.2.1 KP-3-1 ( $\text{Cu}_7\text{In}_3$ )
      - 2.3.2.2 KP-4-1 ( $\text{Cu}_2\text{In}$ )
      - 2.3.2.3 KP-5-1 ( $\text{Cu}_{11}\text{In}_9$ )
- 3 Project progression
  - 3.1 Original time table
  - 3.2 Adjusted time table
- 4 Outlook
- 5 References

## 1. Abstract

The project plan consisted of two main parts, namely the redesign of the in situ methanol steam reforming setup at the beamline 12.2.2 at the Advanced Light Source at the Lawrence Berkeley National Laboratory and the investigation of intermetallic Cu-In phases in methanol steam reforming and potential activation pretreatments.

The planning and the first tests for the vaporizer unit for the MSR setup were completed by the time the LBNL transitioned to a standby mode in accordance with the shelter-in-place order of Alameda county and the City of Berkeley on March 16, 2020. The shelter-in-place order was in effect until the end of the project and I did not have the possibility to enter the lab again to hands-on conduct scientific work and development. Therefore, this part of the project could not be completed.

The second part concerned the investigation of three different intermetallic Cu-In phases in various pretreatments and in MSR before and after these. Three weeks in April 2020 were allocated for these experiments in addition to others in cooperation with researchers from the TU Berlin. Due to the shelter-in-place order, all of this beam time was cancelled and only due to the exceptional efforts of my supervisor and his colleagues, it was possible to perform a small fraction of the experiments remotely. Merely the pretreatments themselves could be executed, because MSR was not possible due to the complexity of the experimental setup and the lack of a proper MSR setup. Therefore, the catalytic performance has to be evaluated separately in the batch reactor at the University of Innsbruck in order to interpret them in a meaningful way.

## 2. Results

The project and any research activity was substantially hampered by the COVID-19 pandemic and the resulting shutdown of the LBNL and the ALS. The shelter-in-place order of the City of Berkeley was in effect from March 16, 2020 until the end of the project. The ALS and the LBNL remained in a standby mode as well in this period. LBNL staff scientists were allowed to enter the ALS for non COVID-related research purposes only in the beginning of June 2020.

The project was not immediately abandoned at the pandemic outbreak due to the ongoing uncertainty and the stepwise development of the shelter-in-place order. It was prolonged several times and it was clear only at the end of May 2020 that I could not perform any experiments at the ALS in person. Thanks to the efforts of my supervisor Martin Kunz and his colleagues, however, I was able to participate in a pilot project for remote user experiments and obtain a small fraction of the anticipated results.

### 2.1 Original goals and research problems

#### 2.1.1 Scientific background

The primary goal of the project was the investigation of three intermetallic CuIn phases in methanol steam reforming (MSR) with in situ X-ray diffraction (XRD). MSR is an important reaction for the reversible storage and release of hydrogen as a carrier of renewable energy. [1] Most of all, the application in the transport sector is promising, because hydrogen can be produced on-board from methanol. The latter is liquid at ambient conditions and, therefore, its storage and distribution is much easier to implement in the existing fuel infrastructure. The hydrogen can then be fed to a proton exchange membrane fuel cell (PEMFC), which provides energy with a higher efficiency than combustion engines. [2]

In order to make MSR feasible on an industrial scale and specifically for the automotive applications, the catalysts for this reaction have to be optimized regarding their activity, long-term stability and CO<sub>2</sub> selectivity. The latter is especially critical for a potential direct use of the reformat in a PEMFC, since even small concentrations of CO can lead to poisoning of the fuel cell electrodes. [3,4]

In the search for materials with these desired properties, knowledge-based approaches are preferable to simple trial and error strategies both considering time and monetary resources. Next to classical heterogeneous powder catalysts consisting of the active component distributed on a support, intermetallic compounds are gaining increased attention as catalytic materials. In the case of MSR, especially Pd-based systems were employed recently. [5–10] However, the interaction with an oxidic support has been theorized to be crucial for the performance of these systems. [11]

There are two main routes to these intermetallic/oxide composite catalysts. Starting from the pure intermetallic compound, (partial) decomposition can lead to the formation of the oxide

component. [12,13] This decomposition can either occur spontaneously in the reaction mixture or be accomplished by specific pretreatments. The other path starts with the preparation of a classical supported powder catalyst (e.g. prepared by wet impregnation) and formation of the intermetallic phase by reactive metal-support interaction. [14]

One oxide that has been shown to display a promising performance in MSR as well as in methanol synthesis by CO<sub>2</sub> hydrogenation is In<sub>2</sub>O<sub>3</sub>. [15,16] Cu, on the other hand, has been implemented in numerous well performing MSR catalyst already. [17] So, the combination of these two materials is a promising start in the search for an effective system. Our workgroup could already show that it is possible to create intermetallic Cu-In phases with reactive metal-support interaction. [18] In this study, Cu was supported on In<sub>2</sub>O<sub>3</sub> by wet impregnation and the intermetallic phases could be obtained by reduction with H<sub>2</sub>. This catalyst displayed an improved activity at a high CO<sub>2</sub> selectivity in comparison with metallic copper on In<sub>2</sub>O<sub>3</sub>.

This project part revolves around the second route to these intermetallic/oxide catalysts. The starting points are three intermetallic Cu-In phases with different stoichiometries (see Table 1 and the phase diagram in Figure 1). Cu<sub>7</sub>In<sub>3</sub> is a triclinic, room temperature stable phase, the high-temperature phase Cu<sub>2</sub>In exhibits a hexagonal structure and the In-richest phase Cu<sub>11</sub>In<sub>9</sub> crystallizes in a monoclinic structure. [19–22] The XRD patterns of all three phases display similar characteristics due to their similar structures and the main reflections of all phases overlap considerably. This renders the differentiation and assignment of the phases a rather challenging task.

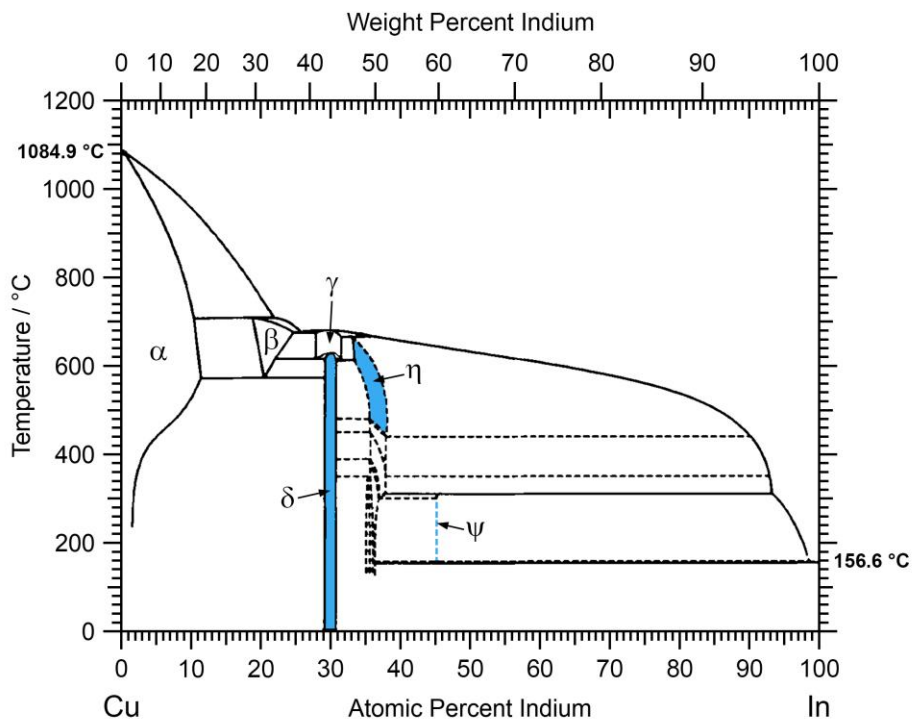


**Figure 1:** Cu-In phase diagram adapted from Subramanian et al. with the synthesized phases marked in blue. [19]

Table 1: List of the samples that were investigated in the project.

| Sample name | Phase acronym | Nominal stoichiometry       |
|-------------|---------------|-----------------------------|
| KP-3-1      | $\delta$      | $\text{Cu}_7\text{In}_3$    |
| KP-4-1      | $\eta$        | $\text{Cu}_2\text{In}$      |
| KP-5-1      | $\psi$        | $\text{Cu}_{11}\text{In}_9$ |

The samples for this project were prepared in cooperation with the workgroup of Prof. Marc Armbrüster at the Technical University of Chemnitz prior to the research stay. The metallic educts, Cu and In, were weighed and mixed according to their stoichiometry in a glove box to prevent oxidation. They were transferred to quartz ampules, which can be evacuated with a turbomolecular pump to a final pressure of approximately  $10^{-5}$  mbar. With a hydrogen/oxygen flame, these quartz ampules are sealed off, which prevents oxidation in the following annealing treatment.

According to the phase diagram, [19]  $\text{Cu}_7\text{In}_3$  is the only room temperature stable intermetallic phase of copper and indium apart from the  $\alpha$ -phase, which can be described as a Cu-rich Cu-In alloy displaying the structure of pure copper. For the synthesis of single-phase products, the mixtures have to be annealed at a temperature approximately 20 °C below their upper stability limit. In this process, it has to be assured that the possibility for diffusion is high enough for the thermodynamically stable phases to form. This means that the lower the temperature of the upper stability limit is, the longer the sample has to be kept at that temperature.

Therefore,  $\text{Cu}_7\text{In}_3$  was annealed at 600 °C for 30 days,  $\text{Cu}_2\text{In}$  at 270 °C for 90 days and  $\text{Cu}_{11}\text{In}_9$  at 270 °C for 90 days. After the annealing, the samples are quenched in ice water to prevent the high-temperature phases from transforming into the respective stable room temperature phases. The quartz ampules can then be crushed and the samples are ground in a mortar for further analysis and catalytic testing.

The project plan revolved around two main subprojects: a) the redesign of the MSR setup at the beamline 12.2.2 at the ALS and b) the investigation of three intermetallic Cu-In phases in various pretreatments and MSR with in situ XRD.

### 2.1.2 Redesign of the MSR setup

The original setup at the beamline 12.2.2 at the ALS was mainly designed for studies on powder samples in various gas environments at elevated temperatures. [23,24] A gas supply system with mass flow controllers delivers a steady stream of the educts or inert gas to the sample located in a quartz capillary. This creates quasi-flow conditions at the sample, since it is located at the bottom of the capillary and the gas flows in and out at its top. A SiC sleeve around the capillary allows for uniform heating of the sample with an infrared lamp up to 1100 °C. [23]

It was possible to conduct MSR with this setup by passing He as a carrier gas through a boiled solution of methanol and water and feeding it into the sample capillary. Because the gas phase is saturated with the mixture at its boiling temperature, it can condense along the way to the sample at any colder spot. This can not only change the composition of the gas phase mixture by preferential condensation of water due to its higher boiling point, but also leads to the formation of droplets in the lines, causing buildup of pressure and potentially exposing the sample to the liquid phase, especially at low specimen temperatures.

Therefore, a vaporization unit should be designed including heated lines up to the sample capillary. Additionally, the composition of the gas phase should be precisely controllable by adaption of the liquid phase composition, since the setup is designed to ensure quantitative evaporation to ensure that the composition of the gas phase is equal to the one of the liquid phase (assuming the applicability of the ideal gas law). The degree of saturation of the carrier gas also needs to be controlled in order to prevent condensation in cold spots.

### 2.1.3 In situ XRD investigations of Cu-In samples in MSR

The major part of the project consisted of the investigation of three previously synthesized intermetallic Cu-In samples. They were tested in MSR and by ex situ XRD before the research stay and their structural evolution in MSR and different pretreatments was to be characterized. The advantage of synchrotron radiation opposed to a laboratory X-ray source is its much higher brightness, which leads to a very high signal-to-noise ratio. This is especially advantageous for the identification of minor phases that would not even be visible with conventional sources.

Since intermetallic phases prepared by co-melting and annealing have a rather low surface area after grinding, they usually have to be activated and/or partially decomposed to increase the activity and potentially also the selectivity. In some systems, like Cu-Zr, this decomposition occurs spontaneously in the MSR mixture, yielding a highly active and CO<sub>2</sub>-selective state consisting of metallic copper and both monoclinic and tetragonal zirconia. [12,13]

In the Cu-In system, this decomposition is much less pronounced and the activity remains comparably low. Therefore, one of the goals was to identify an effective pretreatment for the activation of the samples by selected oxidation potentially in combination with an additional reduction step before MSR. In situ XRD enables direct observation of the bulk structural evolution of the samples and allows its correlation with the catalytic performance in MSR. Additionally, the behavior in MSR without pretreatments was planned to be studied, where the high brightness would be far more suitable for the detection of tiny changes of the diffraction patterns.

At a synchrotron user facility, only a very limited amount of time is granted for each research group to conduct their experiments. In cooperation with the TU Berlin, we were assigned three weeks of shared beam time in April 2020, where the samples of this project would have been characterized together with other samples from our cooperation partner. However, the LBNL including the ALS shifted to a standby mode of operation on March 16, 2020 due to the COVID-19 pandemic. Therefore, the beam time was cancelled entirely and no experiments could be performed on-site.

## 2.2 Changes and deviations

The project plan was completely changed by the impact of the COVID-19 pandemic and the according actions of the local government including the LBNL and the ALS. The latter entered a standby mode in March 16, 2020 that reduced the number of people allowed to work on-site daily from approximately 4500 to 200. The LBNL including the ALS followed the guidelines of the local government of Berkeley, but were also obliged as an institution of the Department of Energy to act in accordance with national decisions. The shelter-in-place order issued by the City of Berkeley was prolonged several times right before it expired, which made it very difficult to decide, whether I should abandon the project prematurely. I decided not to stop, however, because it was still theoretically possible to get beam time up to end of May 2020, at which point the ALS started the planning of the phased reopening with so-called pilot phases. The first one, lasting until beginning of July 2020, did not allow affiliates, my official status during my research stay, to enter the ALS for work. Since the research stay ended on June 12, 2020, this apparently concluded the project.

Despite these difficult circumstances, the whole “Diffraction and Imaging” group including my supervisor Martin Kunz and Andrew Doran, which was mainly responsible to work with me on the redesign of the MSR setup, invested a lot of effort to enable me to perform at least some of the planned experiments. They wrote a proposal for a pilot project for remote user studies in complex experiments and it got approved. Therefore, we received one week of beam time including restarting the equipment and tuning the beam. The experiments could then be performed with either Martin or Andrew on-site and me observing the execution of the measurements and controlling some instruments remotely via “Zoom”.

The concept of the MSR setup was already completed at the time of the issuance of the shelter-in-place order. Most of the parts were purchased and tests were conducted concerning the maximum achievable temperature, the chemical resistance of various components and the heating of the lines. The whole setup could have been assembled and tested two weeks from the lockdown and would have been ready for the beam time in April. But due to the shelter-in-place order and the shift of the ALS to the standby mode, the construction could not be completed.

In the first weeks of the research stay, I started with the familiarization with the beamline 12.2.2 at the ALS by participating in the alignment and tuning of the X-ray beam and some experiments of other users. Additionally, I took some old data measured with the same setup and learned to use the necessary software for processing a 2D detector image to a powder diffraction pattern. To take it even one step further, I taught myself how to perform Rietveld refinements, which allows crystallographic information to be extracted from a powder diffraction pattern.

## 2.3 Summary of obtained results

Only a small fraction of the planned experiments could be conducted due to the COVID-19 pandemic. The ALS was not accessible for affiliates until the beginning of July 2020, and even then, only selected staff were allowed to perform experiments at beamlines. In the following part, the results that were accomplished despite the extremely difficult circumstances, are summarized.

### 2.3.1 MSR setup

The previous setup at the beamline 12.2.2 at the ALS was designed for the utilization of gases at elevated temperatures. Therefore, the introduction of the MSR mixture was a very challenging task and was accomplished by bubbling He through a boiling mixture of water and methanol. The gas phase was saturated with the vapor pressure of the components at the boiling temperature of the mixture, which means that condensation can easily occur at any colder spots on the way to the sample. At certain experiments, the formation of droplets was observed near the catalyst, which has to be avoided.

For these reasons, my supervisor Martin Kunz, Andrew Doran (involved in the design and construction of the previous setup) and I planned a new vaporization unit specifically for providing a controllable amount of vapor with a defined composition in a carrier gas from a liquid mixture. It consists of a syringe pump that precisely controls the flow of the liquid phase down to  $\mu\text{l min}^{-1}$ , a compartment for the quantitative vaporization of the liquid phase including a static gas mixing unit and a heated line system up to the sample capillary.

The required stoichiometry of the gas phase is determined by the molar ratio of the components in the liquid phase. In MSR, a ratio of 1:1 up to 1:2 of methanol:water in the gas phase is commonly employed and both components should be degassed by bubbling with e.g. Ar before mixing, especially for removal of dissolved  $\text{O}_2$  and  $\text{CO}_2$ . The flow of the liquid phase is precisely controlled by a syringe pump and is supplied through a shutoff valve into the vaporization compartment, which is thermally insulated to reach a sufficiently high temperature.

The lines in the box should have a high thermal conductivity to efficiently transfer the heat to the liquid for vaporization. On the other hand, the lines have to be resistant to both methanol, water and potential other reaction mixtures. Both copper and brass have a high thermal conductivity, but could react with the MSR mixture. Stainless steel is more resistant to these chemicals, but has a lower thermal conductivity. For this reason, we set up a corrosion test of copper and brass in methanol, water and a mixture of both right before the weekend after which the ALS entered the standby mode. The choice of material for the lines would have been based on the results of this unfinished corrosion test. The stiffness of the material was another factor to consider for the assembly of the central part of the vaporizer, where a coil has to be wound tightly around a cartridge heater.

The main part of the thermally insulated vaporization unit consists of a cartridge heater (length = 6.5 cm, diameter = 1.3 cm, 300 W), around which the gas line is wound tightly as a coil for efficient

thermal contact. With a 1/8" line, approximately 20 windings corresponding to 100 cm distance in the line must be passed by the liquid, assuring quantitative vaporization. This is especially true since in MSR, only small flow rates of the liquid phase in the range of  $0.01 \text{ ml min}^{-1}$  are required for flow rates of  $5 \text{ ml min}^{-1}$  in the gas phase. Before being loaded onto a He carrier gas stream, complete mixing of the components is accomplished with a static inline tube mixer.

Because the two constituents of the liquid educt mixture might not be evaporated simultaneously, gas bands of almost pure methanol or water could be created. If the flow in the tube is turbulent, mixing of the gases will occur on its own. The Reynolds number describes the regime of laminar and turbulent flow in tubes, where a value of 2900 is given as a lower limit for guaranteed turbulent flow. The estimated value for 1/8" tube diameter and a flow rate of  $5 \text{ ml min}^{-1}$  is 5, which means that the flow would be laminar and mixing has to be assured with special components. For this purpose, a static inline mixer was added to the vaporization unit downstream of the cartridge heater. This element forces the flow to become turbulent with an arrangement of 32 blades that the gas has to pass.

The thoroughly mixed and heated educt gas flow is loaded onto a preheated He carrier gas stream at a T-connection. By tuning the ratio of the He and the liquid mixture flow rate, the concentration of the educts in the stream can be controlled and oversaturation leading to condensation can be prevented. Additionally, the temperature of the gas to the capillary is held above the boiling point of the components with heating tape wrapped around the lines and covered with aluminum foil as well as with a specifically designed heated aluminum block right above the capillary.

For testing of the vaporization unit, anhydrous  $\text{CuSO}_4$  was purchased that changes color from gray to blue upon exposure to water. This was intended as an indicator, if water can successfully be loaded onto the He carrier gas with the setup. As a qualitative proof that  $\text{CO}_2$  is formed and, therefore, MSR performed by the catalyst in the experiments,  $\text{Ba}(\text{OH})_2$  and  $\text{Ca}(\text{OH})_2$  were provided. The aqueous solutions of these chemicals form a white precipitate ( $\text{BaCO}_3$  and  $\text{CaCO}_3$ ) with  $\text{CO}_2$ , which would serve as a proof that the stream coming from the sample contains this product of MSR and the catalyst is active in the experiment.

Unfortunately, the assembly of the setup could not be completed due to the issuance of the shelter-in-place order by the City of Berkeley and the concomitant transition of the LBNL including the ALS to a standby mode of operation.

### 2.3.2 In situ XRD studies

Based on the results of previous investigations of the samples in MSR, no bulk decomposition of the intermetallic phases is induced by the reaction mixture. This is demonstrated by ex situ XRD studies on the samples after MSR up to  $400 \text{ }^\circ\text{C}$  (see Figure 2). Although small changes in the diffractograms are visible before and after catalysis, the goal of this project was the investigation of various pretreatments leading to (almost) complete decomposition of the initial intermetallic phase and their implications for the performance regarding activity and  $\text{CO}_2$  selectivity in MSR.

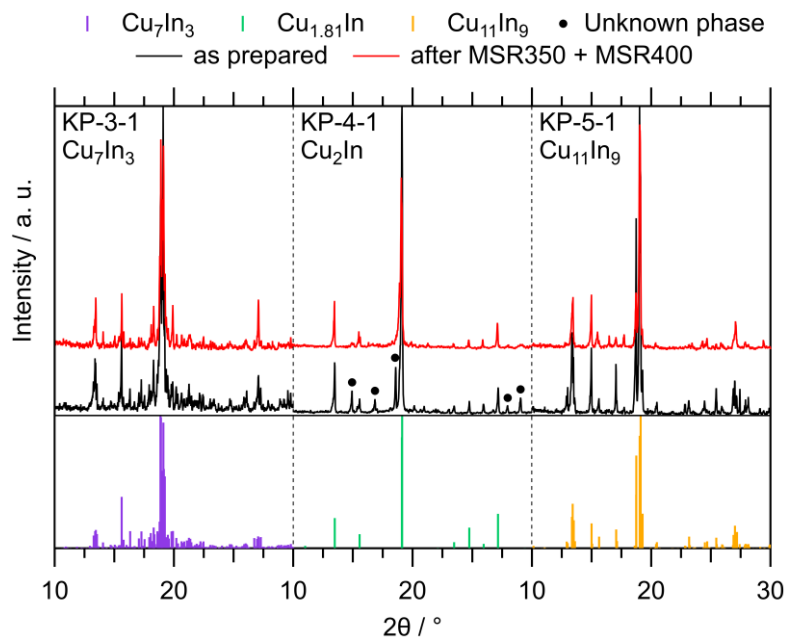


**Figure 2:** Ex situ XRD patterns of the as prepared samples and after two MSR cycles up to 350 and 400 °C. Reference diffractograms were calculated with VESTA [25]:  $\text{Cu}_7\text{In}_3$  [26],  $\text{Cu}_{1.81}\text{In}$  [27],  $\text{Cu}_{11}\text{In}_9$  [22].

However, an interesting fact is the disappearance of the unknown phase in KP-4-1 (marked with black spheres in Figure 2) after MSR, because this sample is the most active without additional pretreatments (see Figure 3). A point to note is that the  $\text{CO}_2$  selectivity of KP-3-1 and KP-5-1 cannot be determined reliably at these low formation rates.

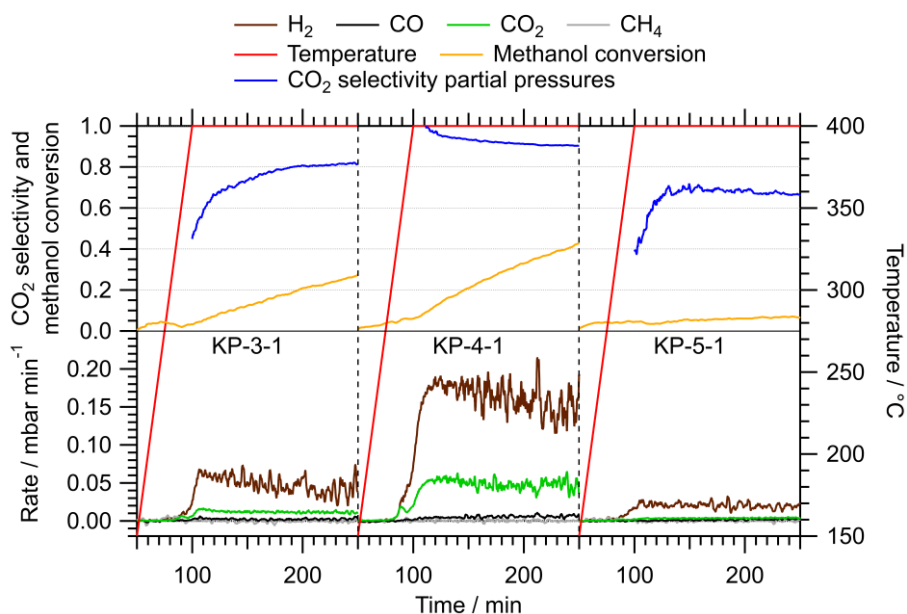


**Figure 3:** Catalytic characterization of the three samples in MSR up to 400 °C in the recirculating batch reactor. In the lower half of the graph, the formation rates of  $\text{H}_2$  (brown),  $\text{CH}_4$  (gray),  $\text{CO}$

(black) and CO<sub>2</sub> (green) are plotted vs. the time. In the upper half, the CO<sub>2</sub> selectivity (blue) and the methanol conversion (orange) are depicted and the temperature is given in red.

For the decomposition of the initial intermetallic phases, an oxidative treatment in 20 vol% O<sub>2</sub> in He was chosen, as similar conditions were tested in thermogravimetric analysis experiments. These indicated almost complete decomposition of the intermetallic phases, which is the goal of this pretreatment. The experiment was initiated at room temperature, followed by a heating ramp of 10 °C min<sup>-1</sup> up to 800 °C, an isothermal period for 30 min and cooling down with 20 °C min<sup>-1</sup> to 20 °C.

In order to assess the impact of an additional reductive treatment on the phase composition and the MSR performance, the samples were exposed to pure H<sub>2</sub> after being oxidatively decomposed. The temperature was increased to 500 °C in hydrogen with a rate of 10 °C min<sup>-1</sup>, followed by an isothermal period of 30 min and cooling down with 20 °C min<sup>-1</sup>.

Each of the two states (after oxidation and after oxidation + reduction) were planned to be investigated with in situ XRD in MSR with the new setup. Due to the complexity of the old setup in conducting experiments involving liquid educts, they could not be performed, since only one beamline scientist was allowed to work at a beamline simultaneously because of the COVID-19 restrictions. The correlation of the pretreatments and the catalytic performance will be accomplished separately by conducting the MSR characterization with the batch reactor setup at the University of Innsbruck after the project.

The raw data obtained at the beamline 12.2.2 of the ALS consists of two-dimensional diffraction images, which were recorded with a newly installed DECTRIS PILATUS3 detector. The exact wavelength of the X-ray beam is calibrated using the NIST LaB<sub>6</sub> 660b standard, which has well known lattice parameters and a defined peak shape. The calibration is performed with the software DIOPTAS [28] that has the literature values of this substance stored in its database. Therefore, the diffraction rings can be selected and the crucial variable parameters like the wavelength and the distance between sample and detector are stored in a calibration file.

In addition to this calibration, regions of the 2D image that are clearly identified as artifacts can be masked and thus excluded from the pattern. Utilizing the mask and the calibration file, DIOPTAS is employed to radially integrate the 2D images to 1D diffraction patterns. These can be arranged in the form of contour plots to show the temperature-dependent evolution of the sample in a 2D graph. For detailed analysis and phase assignment, selected diffraction patterns at special points of interest can be plotted separately.

#### 2.3.2.1 KP-3-1 (Cu<sub>7</sub>In<sub>3</sub>)

Since sufficient decomposition for a high surface area and activity cannot be accomplished in the MSR reaction mixture alone, different pretreatments are investigated and their effect on the bulk structure is studied. The corresponding catalytic characterization has to be conducted separately at the University of Innsbruck, since the COVID-19 restrictions at the ALS did not allow for MSR to be performed at beamline 12.2.2.

The complete oxidation treatment of KP-3-1 is depicted as a contour plot in Figure 4. The intensity is color-coded on a logarithmic scale to ensure the visibility of minority phases. The samples were originally obtained as solid metallic pills with an extremely low surface area. They were crushed in a mortar twice before being measured, but the crystallites were still rather large compared to the 15  $\mu\text{m}$  diameter of the X-ray beam. The resulting lack of powder statistics due to the limited volume of the capillary is apparent in KP-3-1 especially at the start of the treatment. Until the first transformation occurs, the patterns are very spotty.

To compensate the low number of crystallites in the beam, the sample stage is moved periodically in the x and y direction perpendicular to the beam, which travels from negative z to positive z. This procedure enhances the powder statistics considerably by effectively increasing the number of crystallites contributing to the diffraction pattern, but if the position of the sample assembly is not controlled very carefully, the SiC sleeve can touch the incoming X-rays and thus contribute to the diffractogram. Unfortunately, this happened for this sample, which is why SiC is visible in the patterns. Except for the thermal expansions, the related signals remain constant in the experiment. However, the reference for SiC does not fit the corresponding signals perfectly, because it is offset along the X-ray beam relative to the calibrated sample position and both the front or the back wall can be hit. In comparison to the main sample signals, however, the amount of SiC that is visible is very low.

At the start of the experiment, KP-3-1 consists merely of the triclinic intermetallic phase  $\text{Cu}_7\text{In}_3$ , which shows a lot of reflections due to its low symmetry. The first changes are visible at approximately 400  $^\circ\text{C}$ , where  $\text{In}_2\text{O}_3$  starts to be formed. It should be noticed that these reflections are less spotty in their temperature evolution and the diffraction rings in the 2D detector images are very smooth, which means that the crystallites formed are much smaller than those of the original intermetallic phase. The amount of  $\text{In}_2\text{O}_3$  increases up to the isothermal period, from where it stays constant until the end of the experiment.

An interesting phenomenon can be observed at the same temperature of 400  $^\circ\text{C}$ , where metallic copper is formed despite the oxidizing gas atmosphere. The corresponding reflections are shifted to smaller diffraction angles with increasing temperature to a much higher degree than what could be ascribed to thermal lattice expansion. This means that the lattice expansion is caused by incorporation of In into the Cu structure and from around 500 to 700  $^\circ\text{C}$ , the phase matches the reference diffractograms of  $\text{Cu}_{0.9}\text{In}_{0.1}$  well. This phase exhibits essentially the same structure as pure metallic copper, but with a larger lattice parameter due to the incorporation of indium. Before being oxidized,  $\text{Cu}_{0.9}\text{In}_{0.1}$  segregates to metallic Cu and  $\text{In}_2\text{O}_3$  around 700  $^\circ\text{C}$ . At the start of the isothermal period, the last remnants of  $\text{Cu}^0$  are oxidized to  $\text{Cu}_2\text{O}$  and  $\text{CuO}$ .

$\text{Cu}_2\text{O}$  can be observed at approximately 700  $^\circ\text{C}$  for the first time and reaches its peak concentration at the start of the isothermal period. Its amount decreases until a stable rest amount remains. The formation of  $\text{CuO}$  is initiated around 700  $^\circ\text{C}$  and its amount reaches its maximum in the middle of the isothermal period (better visible in Figure 5).

The quantitative decomposition of the original phase  $\text{Cu}_7\text{In}_3$  can be observed around 550  $^\circ\text{C}$ . The main reflections at 12.9 $^\circ$  to 13.2 $^\circ$  start to disappear and the intermediary formation of  $\text{Cu}_{0.9}\text{In}_{0.1}$  is visible. Additionally, the background, especially around the main reflections of  $\text{Cu}_7\text{In}_3$ , increases significantly, which hints to partial melting of the intermetallic phase.

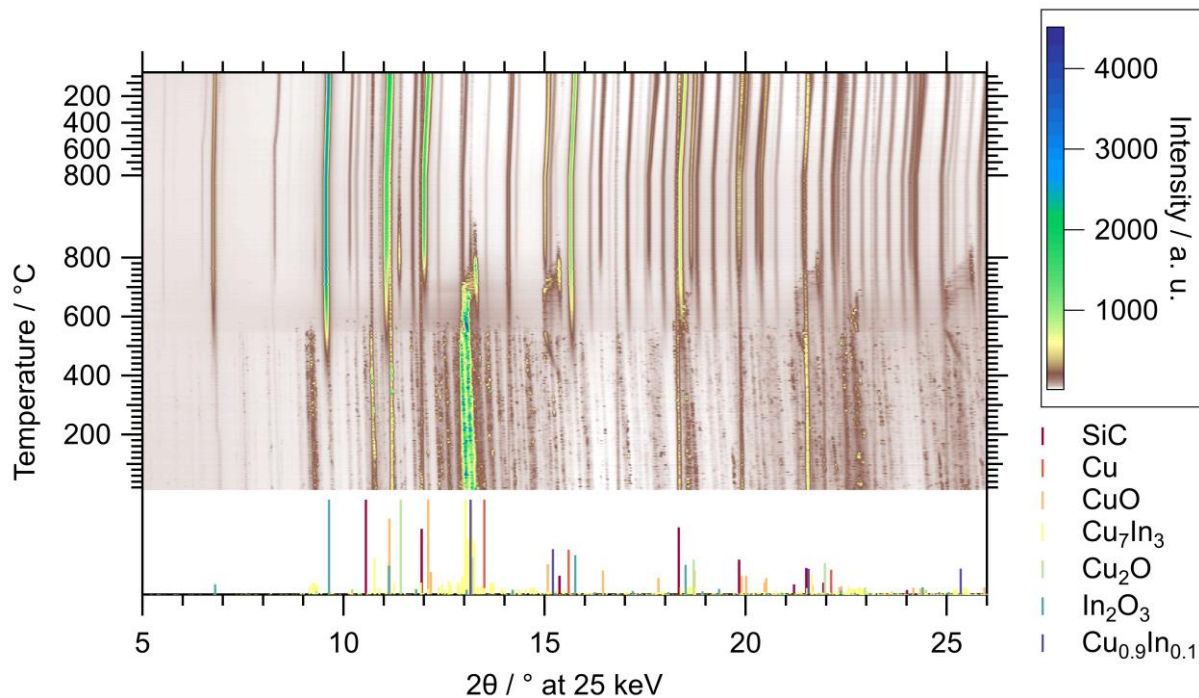


**Figure 4:** In situ XRD patterns in the oxidative treatment of KP-3-1 in 20 vol% O<sub>2</sub> in He from room temperature to 800 °C with a heating ramp of 10 °C min<sup>-1</sup>, followed by an isothermal period of 30 min and cooling down to room temperature with 20 °C min<sup>-1</sup>. The references were calculated with VESTA [25] from the cif-files for the calibrated wavelength of the synchrotron beam: Cu [29], Cu<sub>2</sub>O [30], CuO [31], Cu<sub>7</sub>In<sub>3</sub> [20], Cu<sub>0.9</sub>In<sub>0.1</sub> [32], In<sub>2</sub>O<sub>3</sub> [33] and SiC [34].

Four selected diffractograms of the oxidation of KP-3-1 are depicted in Figure 5. The pattern of the freshly loaded sample only shows the reflections of Cu<sub>7</sub>In<sub>3</sub> and small reflections of SiC due to hitting the heating sleeve with the X-ray beam. At the end of the heating ramp, a small fraction of Cu<sub>7</sub>In<sub>3</sub> remains and the main phases present are In<sub>2</sub>O<sub>3</sub>, Cu<sub>2</sub>O, CuO and Cu<sub>0.9</sub>In<sub>0.1</sub>. CuO is the major copper phase that is present after the isothermal period (besides traces of Cu<sub>2</sub>O) in addition to In<sub>2</sub>O<sub>3</sub> as the sole indium phase. The diffraction pattern is basically unchanged during cooling except for thermal contraction and the concomitant shifts of the diffraction peaks. These shifts can be different for the various phases, since they depend on the thermal expansion coefficient of the crystal structure. Another potential effect is the thermally induced expansion/contraction of the SiC tube and the hole the X-ray beam has to pass through. Since the central position of the sample during the measurement remains the same, the expansion at higher temperature should reduce the intensity of the SiC reflections slightly and vice versa.

The results of the oxidation pretreatment of KP-3-1 clearly show that complete oxidative decomposition can be accomplished with 20 vol% O<sub>2</sub> in He with a maximum temperature of 800 °C. Since the focus of this study lies on intermetallic Cu-In phases, an additional reductive pretreatment is investigated according to the potential reformation of these phases.

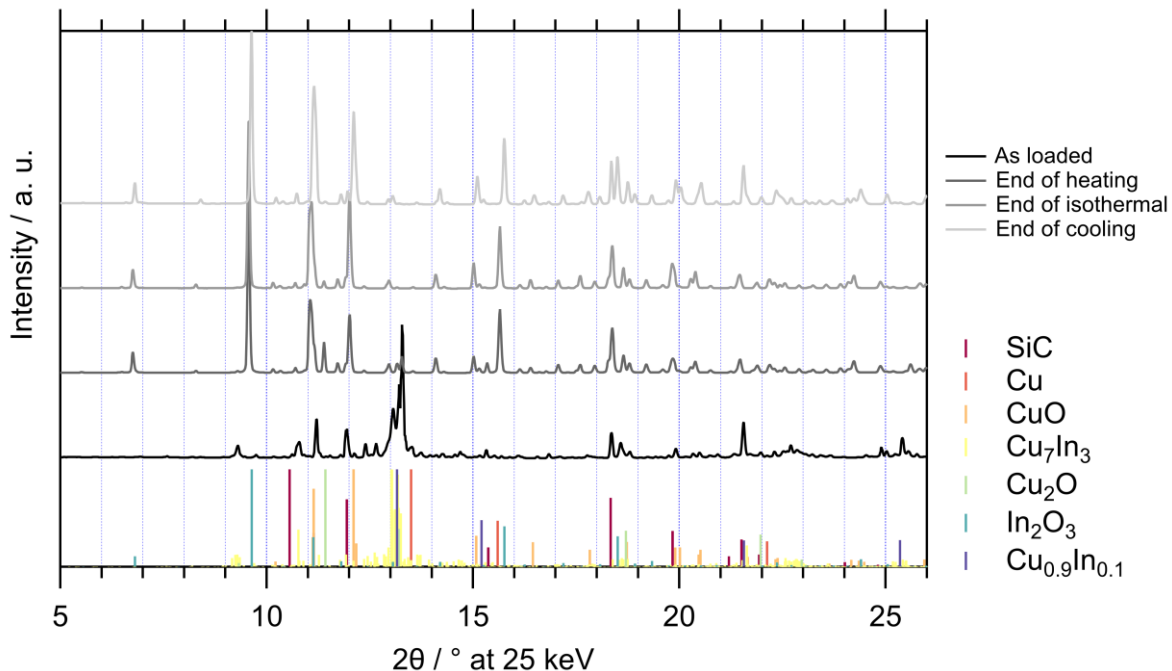


**Figure 5:** Selected diffractograms of KP-3-1 in the oxidation treatment in 20 vol% O<sub>2</sub> in He from room temperature up to 800 °C. The graph depicts the diffraction patterns as loaded, at the end of the heating, isothermal and cooling period, respectively. The references are identical to the ones in Figure 4.

The reduction pretreatment of the oxidized KP-3-1 sample in pure H<sub>2</sub> up to 500 °C is illustrated in Figure 6. The starting state consists of In<sub>2</sub>O<sub>3</sub> as the indium phase and a mixture of Cu<sub>2</sub>O and CuO as the copper phases. The concerted transformation starts at 350 °C with the reduction of both copper oxides to metallic copper. Shortly before the start of the isothermal period, the Cu<sup>0</sup> reflections begin to separate into two peaks. One is the remaining pure metallic copper and the other one shifts to smaller angles by incorporation of In. At the end of the isothermal period, the reflections fit the reference for Cu<sub>0.9</sub>In<sub>0.1</sub> well (also considering the thermal expansion). The decrease of In<sub>2</sub>O<sub>3</sub> is barely visible, because the intermetallic phase that forms has a lower indium content than the original Cu<sub>7</sub>In<sub>3</sub> and some metallic copper remains in its pure form.

Upon cooling, the reflections of Cu<sub>0.9</sub>In<sub>0.1</sub> rapidly shift to larger diffraction angles, indicating segregation of In from the original phase. Simultaneously, the reflections of the pure metallic copper start to broaden and shift towards the peaks of Cu<sub>0.9</sub>In<sub>0.1</sub>. This behavior can be interpreted as an intermixing of Cu<sub>0.9</sub>In<sub>0.1</sub> and Cu and the region between the two limiting phases represents a continuous variation of the lattice parameter caused by the according change of the In content. Additionally, a very broad reflection appears at around 11.4°, which could be assigned to small crystallites of Cu<sub>2</sub>O.

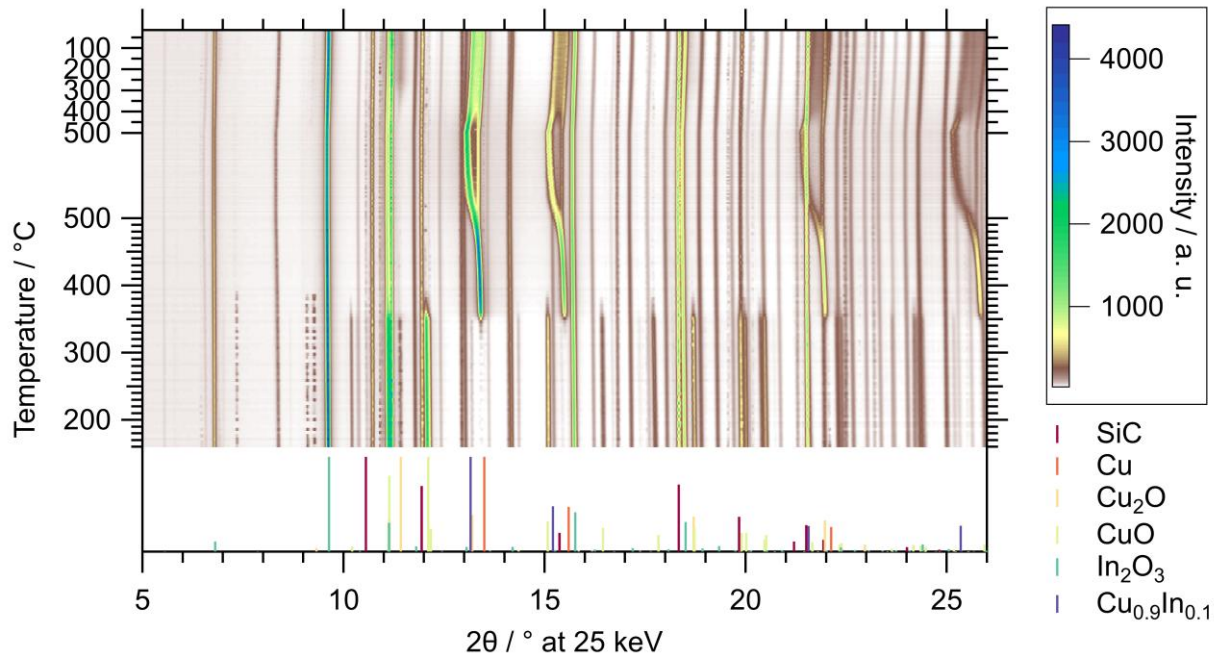


**Figure 6:** In situ XRD patterns in the reductive treatment of KP-3-1 in pure H<sub>2</sub> from 150 to 500 °C with a heating ramp of 10 °C min<sup>-1</sup>, followed by an isothermal period of 30 min and cooling down to room temperature with 20 °C min<sup>-1</sup>. The references were calculated with VESTA [25] from the cif-files for the calibrated wavelength of the synchrotron beam: Cu [29], Cu<sub>2</sub>O [30], CuO [31], Cu<sub>0.9</sub>In<sub>0.1</sub> [32], In<sub>2</sub>O<sub>3</sub> [33] and SiC [34].

The composition of the starting point is confirmed by the diffraction pattern in Figure 7, which consists of In<sub>2</sub>O<sub>3</sub>, Cu<sub>2</sub>O, CuO and the artifacts of the SiC tube. At the end of the heating ramp, the copper oxides have been converted to metallic copper, which starts to incorporate the first In. This process continues in the isothermal period and at its end, the sample is composed of the remaining In<sub>2</sub>O<sub>3</sub> and the well separated phases Cu and Cu<sub>0.9</sub>In<sub>0.1</sub>. Upon cooling, interdiffusion and intermixing of the latter two leads to the formation of a continuous phase distribution with varying In content from pure Cu to Cu<sub>0.9</sub>In<sub>0.1</sub>.

The reductive treatment of the oxidized KP-3-1 sample leads to the reformation of intermetallic Cu-In phases, even though they are different from the initial Cu<sub>7</sub>In<sub>3</sub>. Most of the In<sub>2</sub>O<sub>3</sub> formed in the oxidation remains stable in the final state after reduction. The copper phase, however, was converted to metallic copper with varying In content from 0 at% to approximately 0.1 at% while retaining its original crystal structure. The MSR performance of this state will be studied after the project at the University of Innsbruck in the batch reactor.

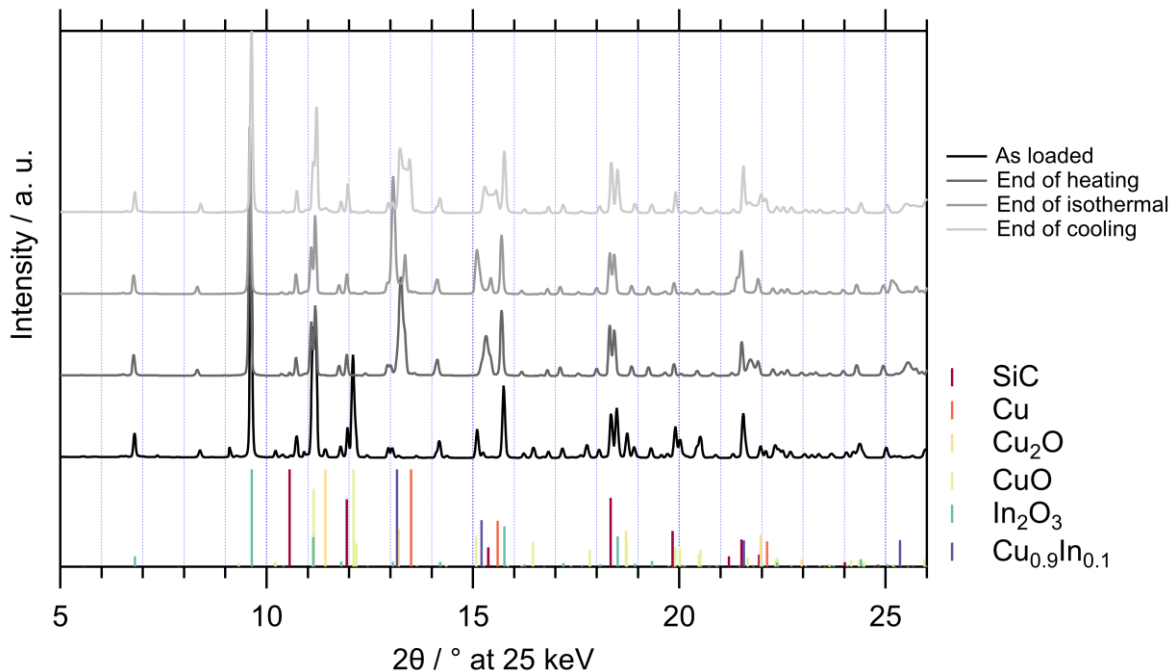


**Figure 7:** Selected diffractograms of KP-3-1 in the reduction in pure H<sub>2</sub> from 150 to 500 °C. The graph depicts the diffraction patterns as loaded, at the end of the heating, isothermal and cooling period, respectively. The references are identical to the ones in Figure 6.

### 2.3.2.2 KP-4-1 (Cu<sub>2</sub>In)

Although partial decomposition of KP-4-1 could already be observed only after conducting MSR up to 400 °C (see Figure 2), the overall activity was still low in comparison to conventional powder catalysts.

The diffractograms of the freshly loaded catalyst exhibit the reflection of a copper-deficient variant of the Cu<sub>2</sub>In high-temperature phase with the same crystal structure, namely Cu<sub>1.568</sub>In. The volume of this phase is slightly lower in comparison to Cu<sub>2</sub>In and the reflections are shifted to higher diffraction angles. Additionally, a yet unidentified phase is present in the sample, but Rietveld refinement for structure determination is an extremely difficult task from a phase mixture. As the η-region in the Cu-In phase diagram features numerous phases and transitions, there might be some unidentified phases in this region.

Around 360 °C, this unidentified phase vanishes and In<sub>2</sub>O<sub>3</sub> starts to be formed. Additionally, the same phenomenon as for the oxidation of KP-3-1 is observable, where traces of metallic copper are formed and immediately In is incorporated accompanied by an expansion of its lattice. Even earlier, around 300 °C, Cu<sub>1.568</sub>In transforms to the triclinic Cu<sub>7</sub>In<sub>3</sub> phase. While the In<sub>2</sub>O<sub>3</sub> content increases steadily up to the beginning of the isothermal period, the newly formed Cu<sub>7</sub>In<sub>3</sub> starts to decompose at approximately 550 °C. The Cu phase reaches its highest In content around the same temperature and starts to decompose to In<sub>2</sub>O<sub>3</sub> and metallic copper. The latter is stable until the start of the isothermal period, where it is converted to Cu<sub>2</sub>O and CuO.

Interestingly, CuO appears already at around 600 °C, but vanishes again briefly at the start of the isothermal period, just to reappear 5 min later. At the same time, Cu<sub>2</sub>O that starts to be visible around 700 °C, has its maximum at this intermediary minimum of CuO. However, Cu<sub>2</sub>O is not oxidized completely and a small amount is stable until the end of cooling.

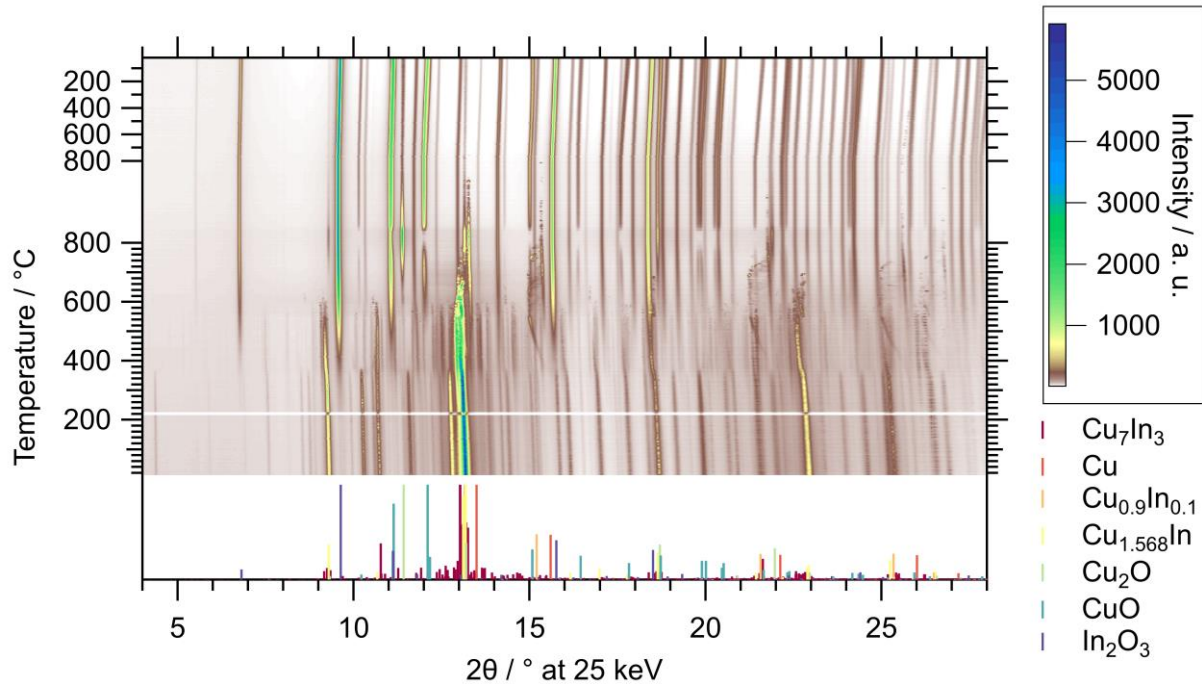


**Figure 8:** In situ XRD patterns in the oxidative treatment of KP-4-1 in 20 vol% O<sub>2</sub> in He from room temperature to 800 °C with a heating ramp of 10 °C min<sup>-1</sup>, followed by an isothermal period of 30 min and cooling down to room temperature with 20 °C min<sup>-1</sup>. The references were calculated with VESTA [25] from the cif-files for the calibrated wavelength of the synchrotron beam: Cu [29], Cu<sub>2</sub>O [30], CuO [31], Cu<sub>0.9</sub>In<sub>0.1</sub> [32], Cu<sub>7</sub>In<sub>3</sub> [20], Cu<sub>1.568</sub>In [35] and In<sub>2</sub>O<sub>3</sub> [33].

The pattern of KP-4-1 as loaded for the oxidation up to 800 °C in 20 vol% O<sub>2</sub> in He is depicted in Figure 9. It is composed of Cu<sub>1.568</sub>In and an unknown phase, which could be an intermetallic Cu-In or even a ternary Cu-In-O phase. At the end of the heating ramp, the original intermetallic phase Cu<sub>1.568</sub>In and the intermediately formed Cu<sub>7</sub>In<sub>3</sub> are already decomposed completely. The sample mainly consists of In<sub>2</sub>O<sub>3</sub>, Cu and Cu<sub>2</sub>O at this point. At the end of the isothermal period, the final composition has already been reached and no further changes are observed upon cooling. The decomposition resulted in the formation of In<sub>2</sub>O<sub>3</sub>, CuO and traces of Cu<sub>2</sub>O.

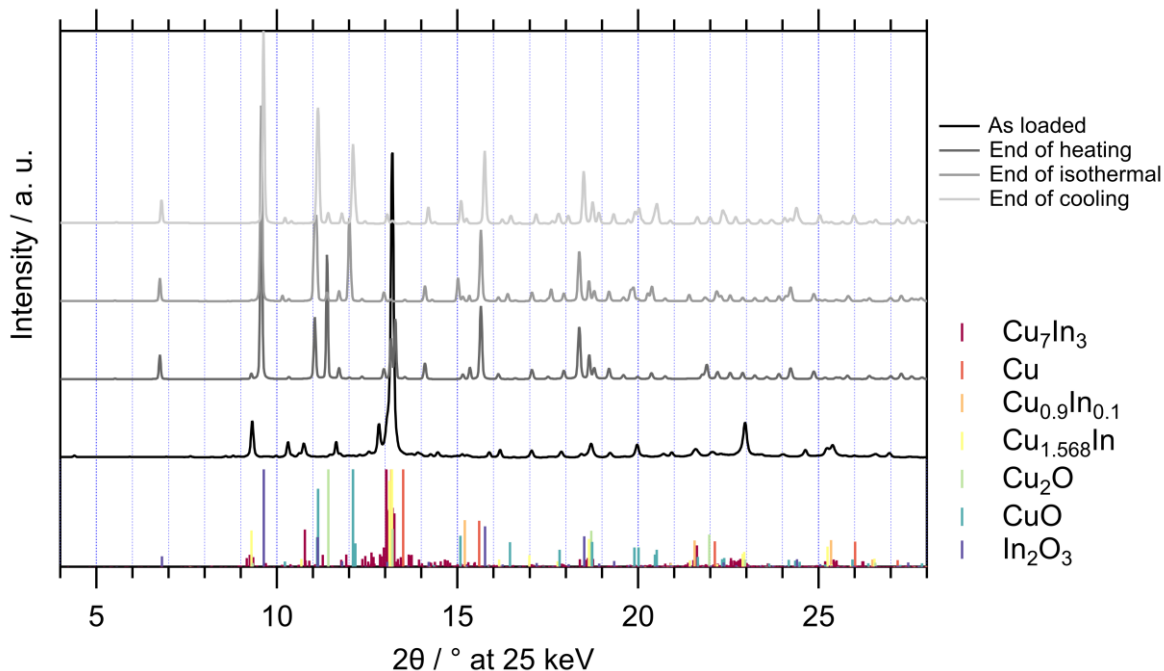


**Figure 9:** Selected diffractograms of KP-4-1 in the oxidation treatment in 20 vol% O<sub>2</sub> in He from room temperature up to 800 °C. The graph depicts the diffraction patterns as loaded, at the end of the heating, isothermal and cooling period, respectively. The references are identical to the ones in Figure 8.

The investigation of the reductive treatment of the oxidized KP-4-1 sample in pure H<sub>2</sub> up to 500 °C is depicted in Figure 10. The initial state consists of In<sub>2</sub>O<sub>3</sub>, CuO and traces of Cu<sub>2</sub>O and at 180 °C, metallic copper starts to be formed. The amount of Cu<sup>0</sup> reaches its maximum at approximately 280 °C, which coincides with the disappearance of both Cu<sub>2</sub>O and CuO. At around 400 °C, incorporation of indium into the pure copper phase is initiated, which ends upon reaching 500 °C and results in a stoichiometry that contains less indium than Cu<sub>0.9</sub>In<sub>0.1</sub>, since the shift to lower angles is too small for this ratio. At that point, a decrease of the In<sub>2</sub>O<sub>3</sub> reflections is observable accompanied by the formation of Cu<sub>7</sub>In<sub>3</sub>. Successively, also the indium-deficient analogue of Cu<sub>0.9</sub>In<sub>0.1</sub> is converted to Cu<sub>7</sub>In<sub>3</sub> in the first half of the isothermal period. The reflections of the freshly formed Cu<sub>7</sub>In<sub>3</sub> still shift to smaller diffraction angles (i.e. larger lattice parameters) despite the temperature being constant. This indicates successive incorporation of In provided by the reduction of In<sub>2</sub>O<sub>3</sub> until the latter reaches its final concentration.

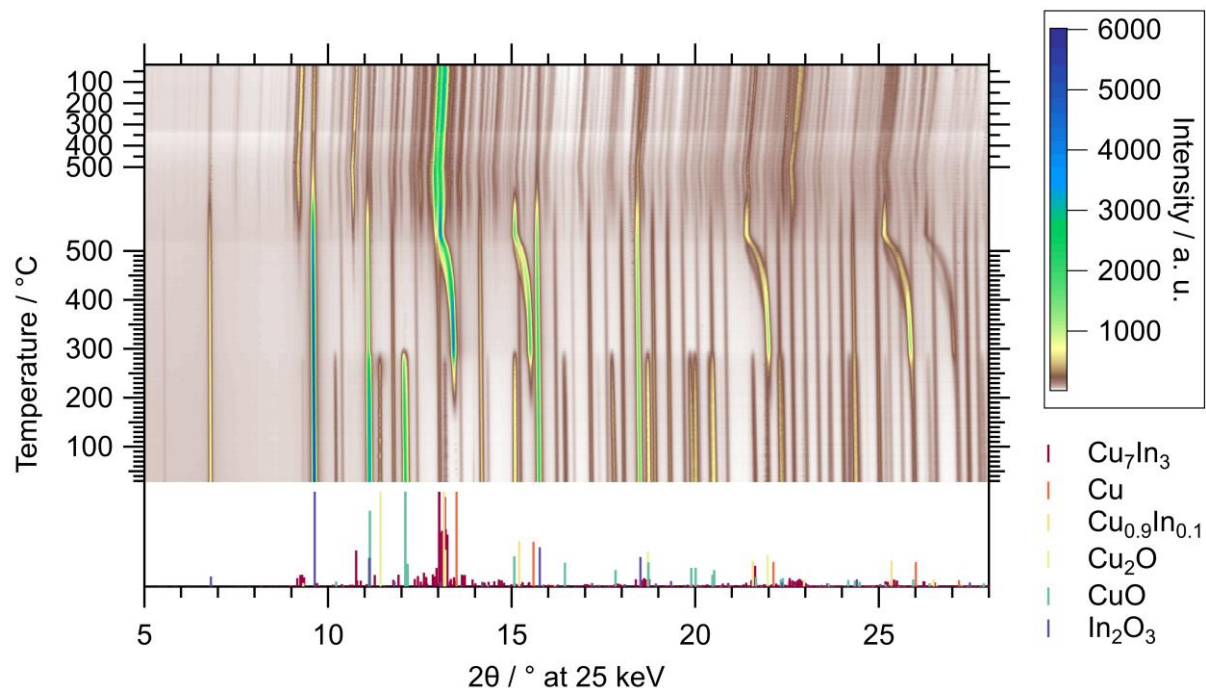


**Figure 10:** In situ XRD patterns in the reductive treatment of KP-4-1 in pure  $\text{H}_2$  from room temperature to 500 °C with a heating ramp of 10 °C  $\text{min}^{-1}$ , followed by an isothermal period of 30 min and cooling down to room temperature with 20 °C  $\text{min}^{-1}$ . The references were calculated with VESTA [25] from the cif-files for the calibrated wavelength of the synchrotron beam: Cu [29],  $\text{Cu}_2\text{O}$  [30],  $\text{CuO}$  [31],  $\text{In}_2\text{O}_3$  [33],  $\text{Cu}_{0.9}\text{In}_{0.1}$  [32] and  $\text{Cu}_7\text{In}_3$  [20].

The diffraction pattern of the freshly loaded KP-4-1 after the oxidation treatment is illustrated in Figure 11 and it identifies the sample to consist of  $\text{In}_2\text{O}_3$ ,  $\text{CuO}$  and traces of  $\text{Cu}_2\text{O}$ . At 500 °C after the heating ramp, the metallic copper phase has already reached its highest degree of indium incorporation, which is probably lower than 0.1 mol%, because the shift of the Cu reflections to lower diffraction angles is smaller than expected for  $\text{Cu}_{0.9}\text{In}_{0.1}$  (also considering the thermal expansion of the lattice). Additionally, the formation of  $\text{Cu}_7\text{In}_3$  and the decrease of the  $\text{In}_2\text{O}_3$  reflections has just started. At the end of the isothermal period, the sample has already reached its final composition and after cooling down to room temperature, it is composed of  $\text{Cu}_7\text{In}_3$  and residues of  $\text{In}_2\text{O}_3$ .

With the studied pretreatments, the initial  $\text{Cu}_{1.568}\text{In}$  phase including the unidentified component could be decomposed completely to  $\text{In}_2\text{O}_3$ ,  $\text{Cu}_2\text{O}$  and  $\text{CuO}$  by oxidation in 20 vol%  $\text{O}_2$  in He up to 800 °C. Reduction in pure  $\text{H}_2$  at 500 °C lead to the formation of  $\text{Cu}_7\text{In}_3$  and some  $\text{In}_2\text{O}_3$  remained stable in these conditions. Both states will be studied with respect to their catalytic performance in MSR in the batch reactor at the University of Innsbruck.

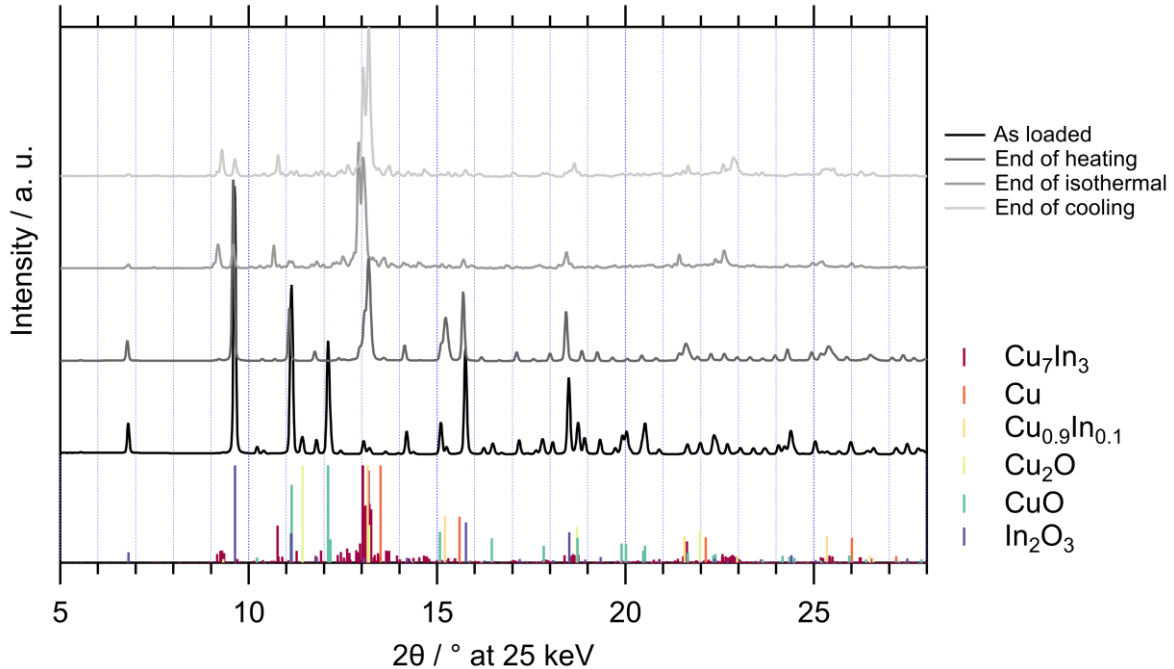


**Figure 11:** Selected diffractograms of KP-4-1 in the reduction in pure H<sub>2</sub> from room temperature to 500 °C. The graph depicts the diffraction patterns as loaded, at the end of the heating, isothermal and cooling period, respectively. The references are identical to the ones in Figure 10.

### 2.3.2.3 KP-5-1 (Cu<sub>11</sub>In<sub>9</sub>)

The oxidation of the sample KP-5-1 in 20 vol% O<sub>2</sub> in He to a final temperature of 800 °C is depicted in Figure 12. Next to the intermetallic phase Cu<sub>11</sub>In<sub>9</sub> small traces of metallic In are visible, which vanish already at 140 °C. At approximately 300 °C, a part of Cu<sub>11</sub>In<sub>9</sub> is transformed to the high-temperature phase Cu<sub>2</sub>In and the rest simply melts, as indicated by the increase in the background around the main reflection of the intermetallic phase. At this temperature, In<sub>2</sub>O<sub>3</sub> starts to be formed, most likely by oxidation of the melt. Another part of the intermetallic phase melts at 490 °C and at around 620 °C, Cu<sub>2</sub>In HT begins to be decomposed, causing an intermediary formation of Cu<sub>2</sub>O. The rest of the intermetallic phase melts at 650 °C and this state is stable in the isothermal period without being oxidized further.

While cooling down, recrystallization sets in at 610 °C, accompanied by an intermediary formation of Cu<sub>2</sub>O. Two different types of intermetallic phases are formed from the melt, namely a low symmetry phase, most likely Cu<sub>7</sub>In<sub>3</sub>, and Cu<sub>0.9</sub>In<sub>0.1</sub>. The former appears at 420 °C while the latter is formed at 560 °C and upon cooling forms a continuous gradient from a stoichiometry of Cu<sub>0.9</sub>In<sub>0.1</sub> to lower indium content, but not to pure metallic Cu, judging by the still visible shift to lower angles relative to Cu<sup>0</sup> at room temperature. Interestingly, no CuO is formed even in these highly oxidizing conditions.

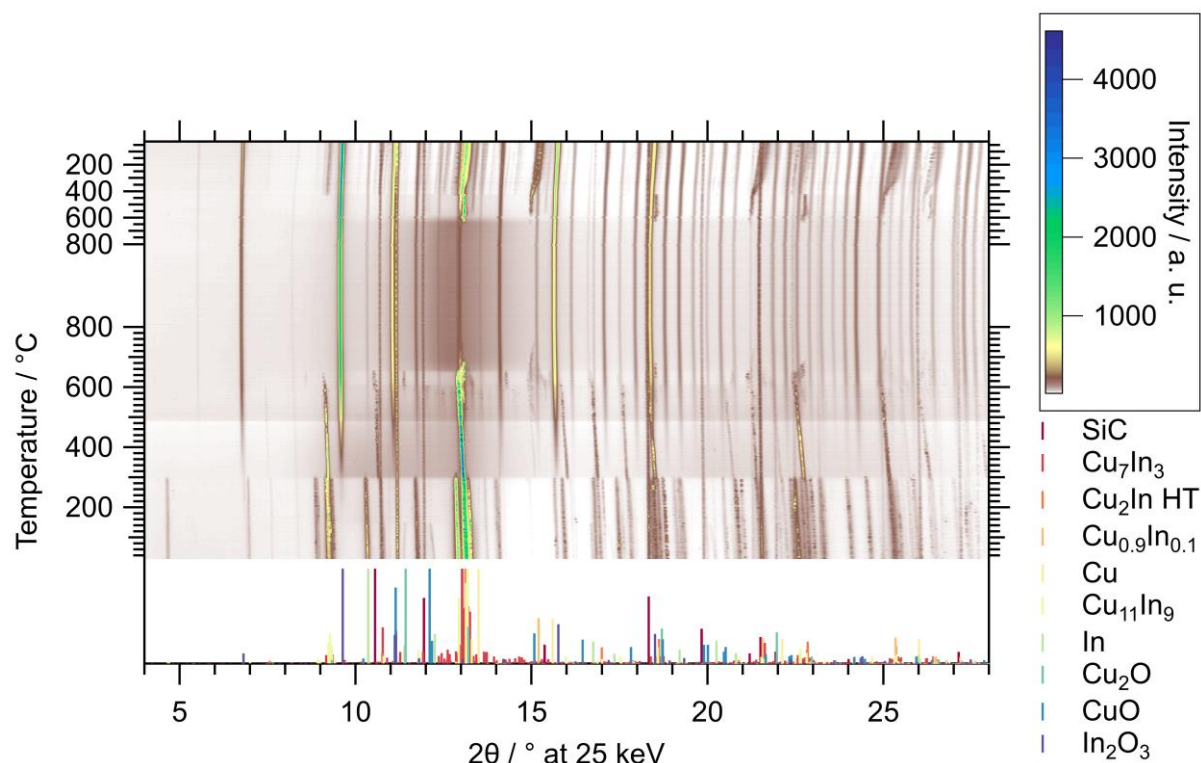


**Figure 12:** In situ XRD patterns in the oxidative treatment of KP-5-1 in 20 vol% O<sub>2</sub> in He from room temperature to 800 °C with a heating ramp of 10 °C min<sup>-1</sup>, followed by an isothermal period of 30 min and cooling down to room temperature with 20 °C min<sup>-1</sup>. The references were calculated with VESTA [25] from the cif-files for the calibrated wavelength of the synchrotron beam: Cu [29], Cu<sub>2</sub>O [30], CuO [31], Cu<sub>11</sub>In<sub>9</sub> [22], Cu<sub>2</sub>In HT [21], Cu<sub>0.9</sub>In<sub>0.1</sub> [32], Cu<sub>7</sub>In<sub>3</sub> [20], In<sub>2</sub>O<sub>3</sub> [33], In [36] and SiC [34].

The diffractogram of the freshly loaded sample KP-5-1 (see Figure 13) consists only of the intermetallic phase Cu<sub>11</sub>In<sub>9</sub>, traces of metallic In and the SiC artifact. At the start of the isothermal period, most of the intermetallic phase has melted and this state is very stable over the course of the isothermal phase. The only other visible component is In<sub>2</sub>O<sub>3</sub> and the diffractogram at the start of cooling is essentially unchanged. After reaching room temperature, two types of intermetallic phases are still present. One is Cu<sub>7</sub>In<sub>3</sub> and the other one encompasses a range of different stoichiometries of Cu<sub>0.9</sub>In<sub>0.1</sub> with the same crystal structure. The only difference between them is a variation of the In content in the lattice, causing it to expand with increasing In incorporation. No pure metallic copper is visible in the final state and no copper oxides like Cu<sub>2</sub>O or CuO are present.

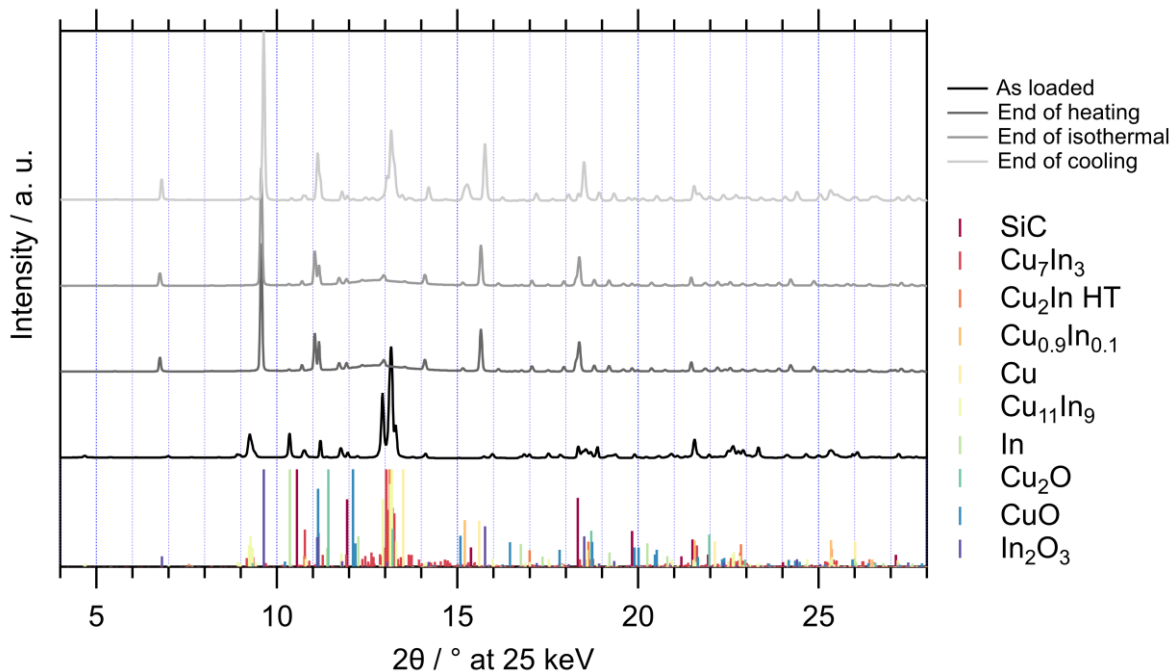


**Figure 13:** Selected diffractograms of KP-5-1 in the oxidation treatment in 20 vol% O<sub>2</sub> in He from room temperature up to 800 °C. The graph depicts the diffraction patterns as loaded, at the end of the heating, isothermal and cooling period, respectively. The references are identical to the ones in Figure 12.

The reductive treatment of the oxidized sample KP-5-1 in pure H<sub>2</sub> up to 500 °C is visualized in Figure 14. The starting diffractogram shows the presence of Cu<sub>7</sub>In<sub>3</sub>, In<sub>2</sub>O<sub>3</sub>, the artifacts of SiC and a range of various stoichiometries of Cu<sub>0.9</sub>In<sub>0.1</sub>, but not including the indium-free phase. In the course of the whole temperature program, only little changes are visible. The major one is the shift of the Cu<sub>0.9</sub>In<sub>0.1</sub>-analogous phases to indium-richer ratios starting around 440 °C, observable as a narrowing of the peak towards lower diffraction angles. This state seems to be stable until the start of the cooling period, where the amount of Cu<sub>7</sub>In<sub>3</sub> increases slightly, leading to a corresponding shift of the Cu<sub>0.9</sub>In<sub>0.1</sub> phases to an overall indium-poorer, yet narrower distribution of copper-indium ratios.

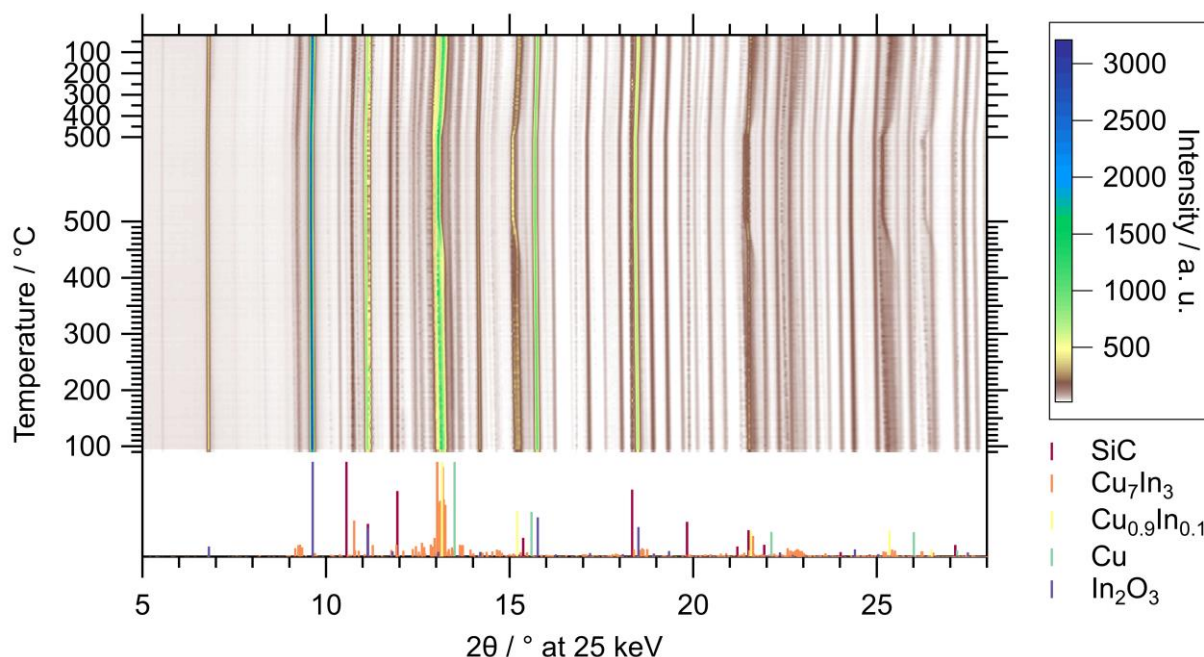


**Figure 14:** In situ XRD patterns in the reductive treatment of KP-5-1 in pure  $\text{H}_2$  from room temperature to 500 °C with a heating ramp of 10 °C  $\text{min}^{-1}$ , followed by an isothermal period of 30 min and cooling down to room temperature with 20 °C  $\text{min}^{-1}$ . The references were calculated with VESTA [25] from the cif-files for the calibrated wavelength of the synchrotron beam:  $\text{Cu}_{0.9}\text{In}_{0.1}$  [32],  $\text{In}_2\text{O}_3$  [33], Cu [29],  $\text{Cu}_7\text{In}_3$  [20] and SiC [34].

The selected diffraction patterns of the reductive treatment of KP-5-1 are depicted in Figure 15.  $\text{Cu}_7\text{In}_3$ , a range of  $\text{Cu}_{0.9}\text{In}_{0.1}$  phases with variable In content,  $\text{In}_2\text{O}_3$  and the artifact reflections of SiC are visible in the pattern of the loaded sample after oxidation. At the end of the heating ramp, the distribution of  $\text{Cu}_{0.9}\text{In}_{0.1}$  stoichiometries has been narrowed down towards In-richer compositions and this state is stable in the isothermal period. The final state after cooling down to room temperature appears very similar to the initial state. Merely the amount of  $\text{Cu}_7\text{In}_3$  increased slightly and the distribution of Cu-In ratios in the  $\text{Cu}_{0.9}\text{In}_{0.1}$  phases became narrower and adjusted to the lower availability of In by shifting to larger diffraction angles due to the contraction of the crystal lattice.

In the sample KP-5-1, no complete decomposition of the intermetallic phases could be accomplished in the selected conditions. Even the molten phases were highly resistant to oxidation and merely recrystallized upon cooling. The successive reduction treatment did not change much either, which means that this copper-indium ratio might not be suitable for activation by decomposition or even harsher conditions have to be applied. Nevertheless, the catalytic MSR performance will be assessed in the batch reactor in both states.

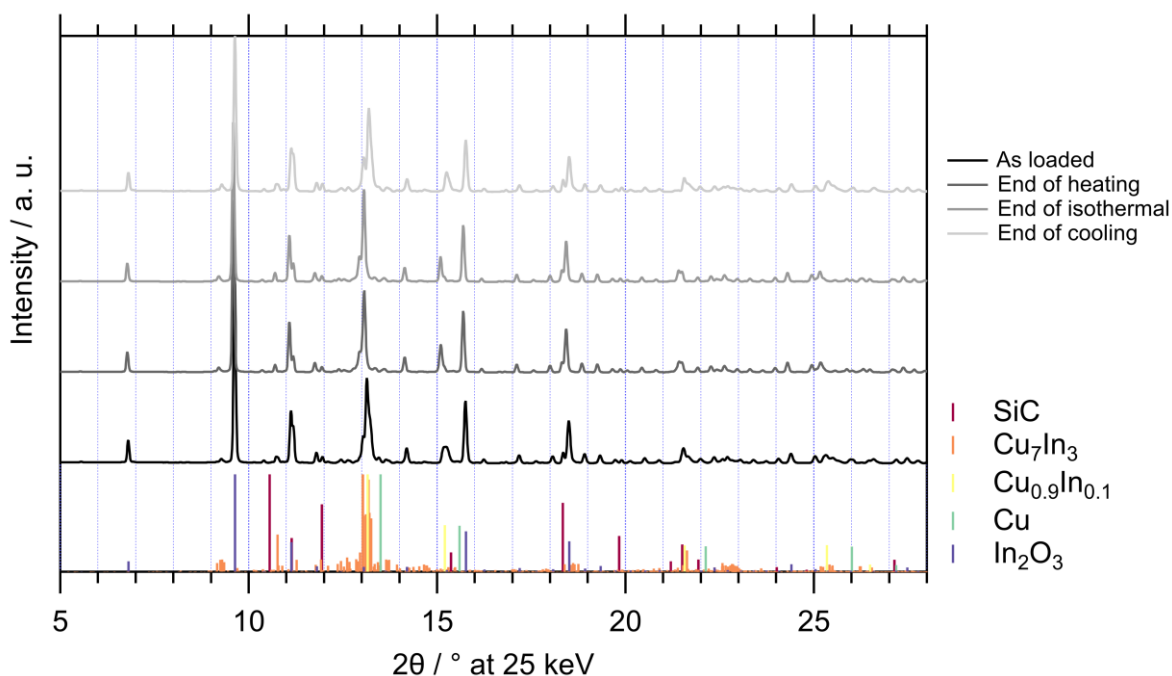


**Figure 15:** Selected diffractograms of KP-5-1 in the reduction in pure H<sub>2</sub> from room temperature to 500 °C. The graph depicts the diffraction patterns as loaded, at the end of the heating, isothermal and cooling period, respectively. The references are identical to the ones in Figure 14.

Summarizing the results of the oxidation and successive reduction of three intermetallic Cu-In samples, considerable differences in their behavior can be observed with in situ XRD.

KP-3-1, consisting only of Cu<sub>7</sub>In<sub>3</sub> at the start, is completely decomposed to In<sub>2</sub>O<sub>3</sub>, Cu<sub>2</sub>O and CuO in the oxidative pretreatment. The reduction of this state leads to the formation of a range of Cu-In phases with a structure analogous to metallic copper, but with varying content of In up to 10 at%. These remain stable upon cooling down to room temperature and a considerable amount of In<sub>2</sub>O<sub>3</sub> is left at the end of the experiment.

Next to Cu<sub>1.568</sub>In, a copper-deficient phase with the same structure as the high-temperature phase Cu<sub>2</sub>In, the sample KP-4-1 contains an additional unassigned phase with a yet unidentified structure. In the oxidation, yields a very similar phase composition as KP-3-1, which consists of In<sub>2</sub>O<sub>3</sub>, CuO and traces of Cu<sub>2</sub>O. The reduction leads to the formation of Cu<sub>7</sub>In<sub>3</sub> next to some remaining In<sub>2</sub>O<sub>3</sub>, but the amount is much smaller compared to KP-3-1, which can be ascribed to the higher indium content of the resulting intermetallic phase.

In contrast to the other two samples, the intermetallic Cu-In phases in KP-5-1, initially composed of Cu<sub>11</sub>In<sub>9</sub> and traces of metallic In, are not decomposed completely to copper and indium oxides in the oxidation. Instead, Cu<sub>11</sub>In<sub>9</sub> is partially converted intermediately and the rest simply melts. In the end, no copper oxides are visible and Cu<sub>7</sub>In<sub>3</sub> next to In<sub>2</sub>O<sub>3</sub> and various Cu<sub>0.9</sub>In<sub>0.1</sub> phases with a range of stoichiometries are formed. This composition barely changes in the reductive treatment, which sets this sample apart from the other two that exhibit similar trends in the investigated pretreatments. The impact of the different structural evolution on the performance in MSR will be evaluated as soon as the according catalytic measurements are finished.

### 3. Project progression

The original time plan for the research stay was divided into four work packages (WPs). They were assigned to the following tasks:

- **WP1:** Sample synthesis, catalytic (batch + flow) characterization in MSR, DTA-TG-MS in MSR, ex situ XRD before and after catalysis
- **WP2:** Familiarization with the setup at the ALS, optimization of MSR at the beamline, planning of the beam time (development of measurement scheme)
- **WP3:** Characterization of the samples by in situ XRD in MSR within the framework of one or two beam times
- **WP4:** Data evaluation and interpretation, planning of additional measurements, preparation of research paper

The WPs were allocated according to the time plan in Figure 16.

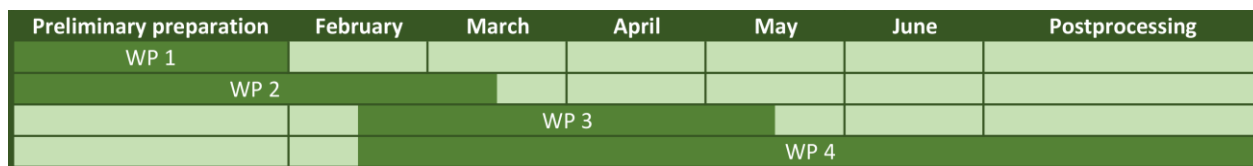


**Figure 16:** The original time plan for the research stay including preparations and post processing.

The only part of the project that was not severely impacted by the COVID-19 pandemic and the concomitant shelter-in-place order is WP 1, which consists of the preliminary preparations. The adjusted time plan in Figure 17 illustrates the WPs that could merely be conducted to a very limited extent or not at all due to COVID-19 restrictions in red. The level of completion of all WPs is as follows:

- **WP1: fully completed;** sample synthesis, catalytic (batch + flow) characterization in MSR, DTA-TG-MS in MSR, ex situ XRD before and after catalysis were successfully executed prior to the research stay
- **WP2: partially completed;** familiarization with the setup at the ALS was close to finished, merely small specific details remained; optimization of MSR at the beamline was in the stage of testing (maximum achievable temperature, chemical resistance of components, heating of gas lines) and assembly, planning of the beam time was in the early stage, since there were three weeks left until the planned start of the beam time
- **WP3: only a small fraction could be completed;** original beam time cancelled entirely; characterization of the samples by in situ XRD could only be performed after the official research stay in a remote fashion; due to the increased complexity of the MSR setup compared to only using gases like O<sub>2</sub>, H<sub>2</sub> and He, only pretreatments could be conducted
- **WP4: only a small fraction could be completed;** data evaluation pathway was developed and refined; only very little data could be obtained and the most relevant part (MSR) could not be performed; evaluation of the data has been conducted; planning of additional measurements including XPS and TEM, preparation of research paper was completed despite the limited amount of data that could be obtained

| Preliminary preparation | February | March | April | May | June | Postprocessing |
|-------------------------|----------|-------|-------|-----|------|----------------|
| WP 1                    |          |       |       |     |      |                |
| WP 2                    |          |       |       |     |      |                |
|                         |          |       | WP 3  |     | WP 3 |                |
|                         |          |       |       |     | WP 4 |                |

**Figure 17:** The adjusted time plan for the research stay. WPs and time periods influenced by the COVID-19 pandemic have been highlighted in red.

## 4. Outlook

The redesign as the first part of the project can be completed as soon as the ALS returns to a normal mode of operation by Martin Kunz and Andrew Doran with the planning and testing conducted during the research stay. The requirements for the assembly of the first prototype have been provided and the setup is expected to significantly improve the reliability and variability of experiments involving the use of gasified liquids as educts at the beamline 12.2.2 at the ALS.

Despite the severely reduced number of experiments that could be performed considering the COVID-19 restrictions, the research stay yielded valuable information on the behavior of three different intermetallic Cu-In samples in oxidative and reductive pretreatments for activation. The impact on their catalytic performance in MSR will be evaluated and correlated with these results by reproducing the same pretreated samples at the University of Innsbruck and conducting catalytic testing in the batch reactor setup. Additional methods will be employed for the characterization of the samples, including X-ray photoelectron spectroscopy and transmission electron microscopy, for further investigation of the structure-activity relationships in the Cu-In system in MSR. These results will enable an efficient and knowledge-based approach for the optimization of these catalysts, thus contributing to the effective storage and distribution of renewable energy in the form of the chemical carrier molecule methanol and the successive release of hydrogen for various applications.

## 5. References

- [1] G.A. Olah, Beyond Oil and Gas: The Methanol Economy, *Angew. Chem. Int. Ed.* 44 (2005) 2636–2639.
- [2] Y. Wang, D.F. Ruiz Diaz, K.S. Chen, Z. Wang, X.C. Adroher, Materials, technological status, and fundamentals of PEM fuel cells – A review, *Mater. Today* 32 (2020) 178–203.
- [3] K. Narusawa, M. Hayashida, Y. Kamiya, H. Roppongi, D. Kurashima, K. Wakabayashi, Deterioration in fuel cell performance resulting from hydrogen fuel containing impurities: poisoning effects by CO, CH<sub>4</sub>, HCHO and HCOOH, *JSAE Review* 24 (2003) 41–46.
- [4] H. Purnama, T. Ressler, R.E. Jentoft, H. Soerijanto, R. Schlögl, R. Schomäcker, CO formation/selectivity for steam reforming of methanol with a commercial CuO/ZnO/Al<sub>2</sub>O<sub>3</sub> catalyst, *Appl. Catal., A* 259 (2004) 83–94.
- [5] M. Friedrich, D. Teschner, A. Knop-Gericke, M. Armbrüster, Influence of bulk composition of the intermetallic compound ZnPd on surface composition and methanol steam reforming properties, *J. Catal.* 285 (2012) 41–47.
- [6] M. Armbrüster, M. Behrens, F. Cinquini, K. Föttinger, Y. Grin, A. Haghofer, B. Klötzer, A. Knop-Gericke, H. Lorenz, A. Ota, S. Penner, J. Prinz, C. Rameshan, Z. Révay, D. Rosenthal, G. Rupprechter, P. Sautet, R. Schlögl, L. Shao, L. Szentmiklósi, D. Teschner, D. Torres, R. Wagner, R. Widmer, G. Wowsnick, How to Control the Selectivity of Palladium-based Catalysts in Hydrogenation Reactions, *ChemCatChem* 4 (2012) 1048–1063.
- [7] H. Lorenz, C. Rameshan, T. Bielz, N. Memmel, W. Stadlmayr, L. Mayr, Q. Zhao, S. Soisuwan, B. Klötzer, S. Penner, From Oxide-Supported Palladium to Intermetallic Palladium Phases, *ChemCatChem* 5 (2013) 1273–1285.
- [8] M. Armbrüster, Intermetallic Compounds in Catalysis, in: I. Horváth (Ed.), *Encyclopedia of Catalysis*, Wiley, 2011.
- [9] N. Iwasa, S. Masuda, N. Ogawa, N. Takezawa, Steam reforming of methanol over Pd/ZnO, *Appl. Catal., A* 125 (1995) 145–157.
- [10] N. Iwasa, T. Mayanagi, N. Ogawa, K. Sakata, N. Takezawa, New catalytic functions of Pd–Zn, Pd–Ga, Pd–In, Pt–Zn, Pt–Ga and Pt–In alloys in the conversions of methanol, *Catal. Lett.* 54 (1998) 119–123.
- [11] M. Friedrich, S. Penner, M. Heggen, M. Armbrüster, High CO<sub>2</sub> selectivity in methanol steam reforming through ZnPd/ZnO teamwork, *Angew. Chem. Int. Ed.* 52 (2013) 4389–4392.
- [12] L. Mayr, B. Klötzer, D. Schmidmair, N. Köpfle, J. Bernardi, S. Schwarz, M. Armbrüster, S. Penner, Boosting Hydrogen Production from Methanol and Water by in situ Activation of Bimetallic Cu–Zr Species, *ChemCatChem* 8 (2016) 1778–1781.
- [13] L. Mayr, N. Köpfle, B. Klötzer, T. Götsch, J. Bernardi, S. Schwarz, T. Keilhauer, M. Armbrüster, S. Penner, Microstructural and Chemical Evolution and Analysis of a Self-Activating CO<sub>2</sub>-Selective Cu–Zr Bimetallic Methanol Steam Reforming Catalyst, *J. Phys. Chem. C* 120 (2016) 25395–25404.
- [14] S. Penner, M. Armbrüster, Formation of Intermetallic Compounds by Reactive Metal-Support Interaction, *ChemCatChem* 7 (2015) 374–392.
- [15] H. Lorenz, W. Jochum, B. Klötzer, M. Stöger-Pollach, S. Schwarz, K. Pfaller, S. Penner, Novel methanol steam reforming activity and selectivity of pure In<sub>2</sub>O<sub>3</sub>, *Appl. Catal., A* 347 (2008) 34–42.

- [16] O. Martin, A.J. Martín, C. Mondelli, S. Mitchell, T.F. Segawa, R. Hauert, C. Drouilly, D. Curulla-Ferré, J. Pérez-Ramírez, Indium Oxide as a Superior Catalyst for Methanol Synthesis by CO<sub>2</sub> Hydrogenation, *Angew. Chem.* 128 (2016) 6369–6373.
- [17] S. Sá, H. Silva, L. Brandão, J.M. Sousa, A. Mendes, Catalysts for methanol steam reforming — A review, *Appl. Catal., B* 99 (2010) 43–57.
- [18] K. Ploner, L. Schlicker, A. Gili, A. Gurlo, A. Doran, L. Zhang, M. Armbrüster, D. Obendorf, J. Bernardi, B. Klötzer, S. Penner, Reactive metal-support interaction in the Cu-In<sub>2</sub>O<sub>3</sub> system: intermetallic compound formation and its consequences for CO<sub>2</sub>-selective methanol steam reforming, *Sci. Technol. Adv. Mater.* 20 (2019) 356–366.
- [19] P.R. Subramanian, D.E. Laughlin, The Cu-In (Copper-Indium) System, *Bulletin of Alloy Phase Diagrams* 10 (1989) 554–568.
- [20] S. Lidin, L. Stenberg, M. Elding-Pontén, The B8 type structure of Cu<sub>7</sub>In<sub>3</sub>, *J. Alloys Compd.* 255 (1997) 221–226.
- [21] G.C. Che, M. Ellner, Powder Crystal Data for the High-Temperature Phases Cu<sub>4</sub>In, Cu<sub>9</sub>In<sub>4</sub>(h) and Cu<sub>2</sub>In(h), *Powder Diffr.* 7 (1992) 107–108.
- [22] T.P. Rajasekharan, K. Schubert, Crystal Structure of Cu<sub>11</sub>In<sub>9</sub>, *Zeitschrift für Metallkunde* 72 (1981) 275–278.
- [23] A. Doran, L. Schlicker, C.M. Beavers, S. Bhat, M.F. Bekheet, A. Gurlo, Compact low power infrared tube furnace for *in situ* X-ray powder diffraction, *Rev. Sci. Instrum.* 88 (2017) 13903.
- [24] L. Schlicker, A. Doran, P. Schnepfmüller, A. Gili, M. Czasny, S. Penner, A. Gurlo, Transmission *in situ* and *operando* high temperature X-ray powder diffraction in variable gaseous environments, *Rev. Sci. Instrum.* 89 (2018) 33904.
- [25] K. Momma, F. Izumi, VESTA 3 for three-dimensional visualization of crystal, volumetric and morphology data, *J. Appl. Crystallogr.* 44 (2011) 1272–1276.
- [26] A.S. Koster, L.R. Wolff, G.J. Visser, Structure of Copper–Indium Cu<sub>7</sub>In<sub>3</sub>, *Acta Crystallogr., Sect. B: Struct. Sci.* 36 (1980) 3094–3096.
- [27] F. Laves, H.J. Wallbaum, Über einige neue Vertreter des NiAs-Typs und ihre kristallchemische Bedeutung, *Zeitschrift für angewandte Mineralogie* 4 (1942) 17–46.
- [28] C. Prescher, V.B. Prakapenka, *DIOPTAS* a program for reduction of two-dimensional X-ray diffraction data and data exploration, *High Pressure Res.* 35 (2015) 223–230.
- [29] M.E. Straumanis, L.S. Yu, Lattice parameters, densities, expansion coefficients and perfection of structure of Cu and of Cu–In α phase, *Acta Crystallogr., Sec. A: Found. Crystallogr.* 25 (1969) 676–682.
- [30] A. Kirfel, K. Eichhorn, Accurate structure analysis with synchrotron radiation. The electron density in Al<sub>2</sub>O<sub>3</sub> and Cu<sub>2</sub>O, *Acta Crystallogr., Sec. A: Found. Crystallogr.* 46 (1990) 271–284.
- [31] S. Asbrink, A. Waskowska, CuO: X-ray single-crystal structure determination at 196 K and room temperature, *J. Phys.: Condens. Matter* 3 (1991) 8173–8180.
- [32] S.C. Chatterjee, M.P. Gupta, Lattice parameters of some binary and ternary copper alloys, *J. Appl. Crystallogr.* 8 (1975) 492–493.
- [33] M. Marezio, Refinement of the crystal structure of In<sub>2</sub>O<sub>3</sub> at two wavelengths, *Acta Cryst.* 20 (1966) 723–728.
- [34] H. Schulz, K.H. Thiemann, Structure parameters and polarity of the wurtzite type compounds Si<sub>2</sub>H and ZnO, *Solid State Commun.* 32 (1979) 783–785.
- [35] S. Lidin, S. Piao, Cu<sub>5</sub>In<sub>3</sub>-Cu<sub>3</sub>In<sub>2</sub> Revisited, *Eur. J. Inorg. Chem.* 2018 (2018) 3548–3553.
- [36] H.E. Swanson, R.K. Fuyat, G.M. Ugrinic, *Natl. Bur. Stand.(US) Circ.* 539 1 (1954) 73.